WARWICK
THE UNIVERSITY OF WARWICK

warwick.ac.uk/lib-publications

Development of a novel process for energy and materials recovery in steelmaking slags

Juncheng Li[1], Debashish Bhattacharjee[2], Xiaojun Hu[3], Dianwei Zhang[4], Seetharaman Sridhar[1*] and Zushu Li[1*]

1. WMG, University of Warwick, Coventry, CV4 7AL UK

2. Tata Steel Research & Development, Moorgate, Rotherham, South Yorkshire, S60 3AR UK

3. State Key Laboratory of Advanced Metallurgy, University of Science and Technology Beijing, Beijing 100083, P. R. China

4. Shougang Research Institute of Technology (Technical Centre), Shijingshan District, Beijing 100043. P. R. China

Full Name	Position	Email addresses	Telephone number
Juncheng Li	Research Fellow	j.li.10@warwick.ac.uk	+44(0)24 7652 8655
Debashish Bhattacharjee	Global R&D Director	debashish.bhattacharjee@tatasteel.com	+31(0)251491428
Xiaojun Hu	Professor	huxiaojun@ustb.edu.cn	+86(0)10 6233 4012
Dianwei Zhang	Principal Researcher	zdw8010@126.com	+86(0)10 8829 7678
Seetharaman Sridhar	Professor	s.seetharaman@warwick.ac.uk	+44(0)24 7657 3255
Zushu Li	Principal Research Fellow	z.li.19@warwick.ac.uk	+44(0)24 7652 4706

∗ Correspondences: Professor Sridhar Seetharaman (s.seetharaman@warwick.ac.uk) and Dr Zushu Li (z.li.19@warwick.ac.uk)

Development of a novel process for energy and materials recovery in steelmaking slags

This work aims at gathering fundamental knowledge for the development of a novel process for energy (H_2 gas) and materials (magnetite Fe_3O_4) recovery in hot-steelmaking slags by reacting molten steelmaking slag with steam. Thermodynamic simulation was carried out to calculate the accumulated amount of produced H_2 gas as a function of the volume of H_2O-Ar gas introduced and the precipitated phases of the molten slags during controlled cooling. Laboratory experiments of crystallisation behaviours of molten slags during cooling were visualized in situ through a confocal laser scanning microscope (CSLM), and the cooled slags obtained were characterised by using SEM-EDS and XRD. CCT diagrams for different slags were created showing the slag crystallisation/phase transformation at different cooling rates. The recovery ratio of H_2 gas and the maximum potential recovery ratio of iron oxide in the oxidised slags were calculated, which concludes that with increasing the slag basicity from 1.0 to 1.5 and 2.0, the recovery ratio of H_2 was found to increase from 12.6% to 23.7% and 22.6%, and the maximum potential recovery ratio of iron oxide was found to increase from 18.3% to 34.4% and 32.8% under the investigated conditions.

Keywords: steelmaking slag; H_2 gas; spinel; CCT diagram; recovery

Introduction

The steel industry produces large volumes of waste slag with huge sensible heat (at extremely high temperature >1500°C) and considerable amount of metals (Fe, Mn, V, Cr, Co, Mo etc) in oxide forms. For example, the basic oxygen steelmaking process (BOS process) generates 100 (up to 150) kg slag per tonne liquid steel at temperature up to 1650°C that contains ~25% (20% to 30%) FeO. In 2013, ~1,139 Mt steel was produced via the BOS process worldwide with ~114 Mt waste slag generated. In order to utilise the thermal energy of molten slags, three types of technologies have been reported: heat recovery as hot air or steam (Barati *et al.*, 2011), conversion to chemical energy as fuel (Lee and Sohn, 2014), and thermoelectric power generation (Rowe 2006 and Nomura *et*

al., 2010). Over the past four decades, granulation or quenching processes are in general used for slag cooling, which are not environmentally friendly. However, no process known so far has been commercialised to recover either the huge thermal energy or the valuable metal oxides contained in the waste slags.

Currently the steelmaking slag is mainly applied in civil engineering (especially for road and waterway construction) (Pioro and Pioro, 2004), in agriculture (fertilizer and soil improvement) (Makelaa *et al*., 2012), and as raw materials for cement and concrete (Iacobescua *et al*., 2011), which inevitably not only generates a number of environmental problems (high levels of alkalinity upon dissolution) (Riley and Mayes, 2015), but also leads to the loss of the targeted metals in the oxides form (Semykina, 2012 and Semykina and Seetharaman, 2011a).

Several metallurgical processes have been developed to recycle iron from the slags, such as directly reducing FeO in steelmaking slag by graphite and coal chars (Min *et al*., 1999, Teasdale and Hayes, 2005), smelting reduction of FeO in steelmaking slag by solid carbon (Bhoi *et al*., 2006). However, its implementation is constrained by unavoidable carbon footprint and large energy consumption. An alternative approach involving oxidation of divalent iron (FeO) to trivalent state (Fe_3O_4) in the liquid slags by air and subsequently separating magnetite from the quenched slag by magnetic separation has been proposed by Semykina *et al*. (2010a, 2010b, 2011b,). This promising method may enable efficient selective recovery of transitional metal oxide from steelmaking slags, especially for the $CaO-SiO_2-FeO(-MnO-V_2O_3)$ bearing steelmaking slag. On the other hand, Bhattacharjee *et al*. (2007) and Mukherjee, T. and Bhattacharjee, D. (2007) invented a method for producing hydrogen-rich gas without generating extra CO_2 emissions by using the thermal energy of molten slag from steelmaking. With this method, when water is sprayed on molten slag, thermo-chemical decomposition of steam takes

place on the slag surface. Oxygen from the decomposition of steam is trapped in the slag to react with metal oxides and hydrogen is released as the product gas. Laboratory study on the slag-steam reactions was also reported by Sato *et al.* (2012) and Matsuura and Tsukihashi (2012).

When the steelmaking slag is reacting with the water vapour, the following reactions described in Eq. (1) and Eq. (2) can be expected:

$$2\ FeO\ (l) + H_2O\ (g) = Fe_2O_3\ (s) + H_2\ (g) \qquad (1)$$

$$Fe_2O_3\ (s) + FeO\ (l) = Fe_3O_4\ (s) \qquad (2)$$
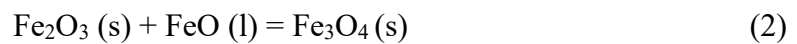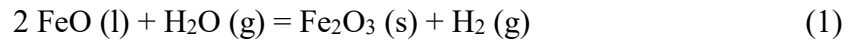
The ultimate aim of the authors in this paper is to develop a novel process for the energy and material recovery in steelmaking slags though integrating the heat recovery process by Bhattacharjee *et al.* (2007) and Mukherjee, T. and Bhattacharjee, D. (2007) with the materials recovery process by Semykina *et al.* (2010a, 2011b, 2012). The technological sheet to effectively utilise steelmaking slag is shown in Fig. 1. Water vapour is introduced to react with the molten slag and produce the environmental-friendly H_2 gas and magnetically susceptible compounds (e.g. magnetite Fe_3O_4) under controlled conditions. When the slag was quenched to the room temperature, the magnetic separation technology was applied to separate the magnetically susceptible compounds and the tailing can be processed to cement (Kourounisa *et al.*, 2007) and concrete (Devia and Gnanavel, 2014).

The main objective of this research is to examine the production of H_2 gas and the generation of magnetically susceptible compounds in the reaction between molten slag and water vapour, and the crystallisation behaviour of the oxidised slags during controlled cooling. The fundamental knowledge created in this study will be employed in the design and optimization of the novel process for energy and materials recovery in steelmaking slags by reacting molten steelmaking slag with steam.

Thermodynamic analysis

Methodology of thermodynamic calculations

The synthetic slags investigated in this work are CaO-SiO_2-FeO-MnO-MgO-Al_2O_3 systems and their designed compositions are shown in Table 1. Prior to laboratory experiments, thermodynamic calculations were performed using FactSage 7.0 (Thermfact and GTT Technologies, Montreal, Canada). As shown in Fig. 2, the calculation comprises three steps of molten slag equilibration in Ar, slag-gas equilibrium, and molten slag solidification in Ar. Firstly, 100 g of synthetic slag was equilibrated at 1600℃ under Ar atmosphere in order to start with a homogenous single molten phase. Then the molten slag was equilibrated with H_2O-Ar gas (0.5 ml, 100°C) resulting in condensed phases and H_2-H_2O-Ar gas. It should be pointed out that H_2O partial pressure in the H_2O-Ar gas at the start point is 1.0 for thermodynamic calculation and the saturated vapour pressure at 60 °C with the Ar flow for the experiment. This slag-gas equilibrium was repeated 200 times until the total volume of H_2O-Ar gas was 100ml. In every calculation all the condensed phases such as molten slag and/or various solids from previous calculation remained in the system as the initial condensed phases in the next calculation and the produced H_2-H_2O-Ar gas from previous calculation was refreshed with H_2O-Ar gas (0.5 ml, 100℃). It was assumed that there was no enthalpy change of the system when 0.5ml of H_2O-Ar gas at 100℃ was equilibrated with condensed phases at each calculation step. Finally, the molten slag and condensed phases in the last calculation step was cooled under Ar atmosphere to obtain magnetically susceptible compounds. For the clarity of explanation, in this paper the slag samples obtained by reacting with H_2O-Ar gas at 1600℃ and subsequently cooling in Ar atmosphere are labelled as oxidised slags while the slag samples obtained by keeping at 1600℃ and then cooling under Ar atmosphere only are

labelled as un-reacted slags.

In this study the commercial thermodynamic package FactSage 7.0 has been used for the purpose of predicting the trends and limits of the related reactions under equilibrium state. As detailed below, the H_2 produced and the slag crystallisation behaviour under equilibrium state have been predicted under varying conditions (the amount of H_2O, slag composition, temperature, etc.). However, in actual process, these reactions are affected by various kinetic factors such as the reaction time, the reaction area of the slag-gas system, etc. This results in the extent of the studied reactions deviated from that predicted by the thermodynamic calculation. The laboratory experiments reported in this manuscript and future work aim to elucidate the effect of the kinetic factors on the H_2 generation and slag crystallisation behaviour in actual process.

Calculation results

Fig. 3 shows the change in the total (accumulated) amount of H_2 gas produced as a function of the volume of H_2O-Ar gas introduced and slag basicity. The accumulated amount of produced H_2 gas increased with increasing the slag basicity (CaO/SiO_2). However, this increase rate decreased when the slag basicity was larger than 1.5. The activity of FeO in the slags investigated in this study can be considered to increase with increasing the slag basicity (Fetters and Chipman 1941, Turkdogan and Pearson 1953), which results in the increase of H_2 gas produced (Reaction (1)). Increasing the basicity of the slags investigated in this work increases the solid fraction of the slag and consequently the FeO in liquid. The latter results in the increased amount of H_2 gas production. On the other hand, the increase in the solid fraction of the slag decreases its fluidity and the Fe^{2+} migration in the slag, which is not beneficial to the generation of H_2 gas. As a result, with increasing the slag basicity, the accumulated amount of produced H_2 gas increased but its

increase rate decreases. Similar trend on H_2 generation was also reported by Sato *et al.* (2012) and Matsuura and Tsukihashi (2012).

Fig. 4 shows the calculated amount of different phases present in the un-reacted slag (B=1.5) at different temperatures. The precipitation sequence of phases was in the descending order of α-Ca_2SiO_4, β-Ca_2SiO_4, monoxide, $Ca_3MgSi_2O_8$, melilite and olivine, with the precipitation starting at temperatures of 1426℃, 1404℃, 1369℃, 1292℃, 1228℃ and 1181℃ respectively. The slag-liquid completely solidified at ~1100℃. The monoxide phase in the un-reacted slag (B=1.5) was, as shown in Fig. 5, 81.90% of FeO and the rest of MnO, MgO and Fe_2O_3. In comparison, the amount of different phases precipitated from the oxidised slag (B=1.5) and the main iron containing components in spinel phase were shown in Fig. 6 and Fig. 7 respectively. The calculated precipitation sequence of phases from oxidised slag (B=1.5) were in the descending order of $CaMgSi_2O_8$, spinel, β-Ca_2SiO_4, melilite, monoxide and olivine, with the precipitation starting at temperatures of 1334℃, 1300℃, 1280℃, 1269℃, 1229℃ and 1160℃ respectively. The slag-liquid solidified at ~1050℃ for the oxidised slag (B=1.5). The spinel phase consists of 72.12% of Fe_3O_4 and the rest of Fe_2O_3-MgO/Al_2O_3. Compared with the precipitated phases of the un-reacted slag (B=1.5), the precipitated temperature of primary phase and the disappearance temperature of the slag liquid decreased for the oxidised slag (B=1.5). This may be attributed to the change of slag composition after reacting with H_2O-Ar gas and the reaction products such as Fe_2O_3 and Mn_2O_3, which decreased the melting temperature of the slag, the precipitation temperatures of different phases and the solidification temperature of the slag liquid. Fig. 8 shows the change in the accumulated amount of spinel phase precipitated from oxidised slags with different basicities. Increasing the slag basicity from 1.0 to 1.5 increased the formation of spinel

phase while the amount of spinel phase decreased when the slag basicity increased from 1.5 to 2.0.

Experimental

Slag Preparation

The designed composition of the synthetic slags investigated in this work was displayed in Table 1. All the slags were made from chemical reagents with a purity of 99.9 wt.%, supplied by Sigma Aldrich. Prior to mixing, the chemical reagents of CaO, SiO_2, Al_2O_3 and MgO were dried at 1000℃ for 4 hours under Ar atmosphere to remove the small amount of volatiles and hydrones. The dry chemical reagent powders were well mixed with FeO and MnO powders based on Table 1, then put into a platinum crucible, and heated in a tube furnace at 1600°C for 1 hour under high purity of Ar atmosphere. The temperature of the tube furnace was controlled by a program controller with an R type thermocouple, within the observed precision range of ±3°C. The pre-melted slag was then rapidly cooled to room temperature. The slag prepared by this procedure was called master slag. The master slags were pulverised and analysed by X-ray fluorescence apparatus (XRF-1800X from Shimadzu Corporation), with the composition shown in Table 2. The composition of the master slags was close to the designed composition of the synthetic slags (Table 1).

Experimental Apparatus and Procedure

Fig. 9 shows the schematic diagram of the experimental apparatus. It consists of moisture generator and confocal laser scanning microscope (CSLM). In the current study, the crystal precipitation event was observed optically in situ under the CSLM and recorded by VTR. The constant H_2O partial pressure was obtained by continuously supplying

argon gas into flasks that was placed inside a heating mantel with the temperature kept at 60℃. The gas tube from the outlet of flask to the inlet of furnace chamber was kept at 60℃ by heating tape. During the experiments the slags were processed through three successive steps: melting at 1600℃ under Ar atmosphere, oxidising under H_2O-Ar atmosphere at 1600℃ for 20 minutes, and quenching under Ar atmosphere. Before introducing the H_2O-Ar gas into the chamber, 0.1 g of the master slag was put into a Pt crucible and then heated at the hot stage of CSLM under Ar atmosphere. To ensure the slag fully melted, the sample was kept at 1600℃ under argon gas for 5 minutes and then the argon gas was switched to H_2O-Ar gas to react with molten slag for 20 minutes at 1600℃. After the oxidising of the molten slag, the H_2O-Ar gas was switched to Ar gas and the slag was quenched. The samples obtained in this process were called oxidised slags. The microstructure and mineral composition of the quenched slags were analysed by electron scanning microscopy (Sigma from Zeiss) equipped with energy-dispersive X-ray spectroscopy (Xmax50 from Oxford Instrument) and XRD (Empyrean from Panalytical) respectively. At the same time, comparison experiments were carried out throughout under Ar atmosphere, with melting at 1600℃ for 25 minutes and then quenching to room temperature. The samples obtained in comparison experiments were called un-reacted slags.

Results and discussion

Crystal observation and phase characterisation

Fig. 10 shows the crystallisation behaviour of the oxidised slag (B=1.5) observed by CSLM at the cooling rate of 10℃/min. Fig. 10(a) and Fig. 10(b) show the morphology of the master slag (B=1.5) at room temperature and at 1600℃ under Ar atmosphere,

respectively. The nucleus of the primary crystal phase was observed to form at 1358℃ (Fig. 10(c)), while the second phase was observed to precipitate at 1233℃ (Fig. 10(d)). With decreasing the temperature, the quantity and volume of the crystal nucleus increased gradually (Fig. 10(e)-10(g)). Finally, the slag liquid was observed to disappear at 1115℃ (Fig. 10(h)) and self-pulverization at 311℃ (Fig. 10(i)). The self-pulverization (Fig. 10(i)) of slag was caused by the phase transformation at ~ 400℃ from β-Ca_2SiO_4 precipitated at high temperature to γ-Ca2SiO4. This phase transformation resulted in the volume increase by >10%, which has already been verified by the studies of Monaco and Lu (1996) and Tossavainen *et al*. (2007). It should be pointed out that the crystallisation temperature of a precipitated phase was assumed to be the temperature when the crystal nucleus first came into the sight under CSLM observation although the crystal nucleus might form ahead of the observation due to the limited resolution of CSLM.

Fig. 11 shows SEM photographs of oxidised slag (B=1.5) at the cooling rate of 10℃/min with different magnification factors. As shown in Fig. 11(b), mainly three phases in the quenched slag were observed, namely the white phase, light grey phase and dark grey phase. In order to determine the elementary distribution in different phase, EDS mapping analysis was employed and the corresponding results were presented in Fig. 12. Ca and Si were mainly enriched in the dark grey phase as matrix phase, while Fe was mainly concentrated in the white phase and light grey phase. Mn is mainly concentrated in the white phase while Al is mainly in the light grey phase. As shown in Table 3, EDS spot analysis indicated that the white phase was close to $Fe_{2.35}MnO_{3.72}$ while the light grey and dark grey phases were approaching $Ca_{2.03}FeO_{4.30}$ and $Ca_{2.01}SiO_{4.23}$ respectively.

Fig. 13 compares the phases present in both the oxidised slag (B=1.5) and un-reacted slag (B=1.5) at the cooling rate of 10°C/min. The main phases in the oxidised slag

were detected to be spinel (magnetite Fe_3O_4) and di-calcium silicate (Ca_2SiO_4) with a small amount of $Ca_2Mn_{0.34}Fe_{1.66}O_5$ and Ca_2FeAlO_5, while the un-reacted slag comprises mainly di-calcium silicate (Ca_2SiO_4), $(MgO)_{0.239}(FeO)_{0.761}$ and $Ca_{2.98}Mn_{0.02}Fe_{1.16}Al_{0.91}Si_{2.93}O_{12}$ with a small amount of Fe_3O_4. By comparing the integrated intensities of the diffraction peaks from each of the known phases, the weight fraction of spinel (magnetite) phase in the oxidised slag and un-reacted slag were semi-quantitatively determined to be 37% and 6% respectively. So the reaction between molten slag and H_2O-Ar gas increased the amount of magnetite phase (Fe_3O_4) by 31 %.

By combining the crystallisation behaviour observed by CSLM, the microstructure analysed by SEM-EDS and the phases present in the slag characterised by XRD, for the oxidised slag (B=1.5), the primary phase formed at 1358℃ (Fig. 10(c)) can be considered as Ca_2SiO_4 and the second phase precipitated at 1233℃ (Fig. 10(d))) can be considered at Fe_3O_4, which is in agreement with the calculation results shown in Fig. 6. The observation results for other oxidised slags and the corresponding un-reacted slags were similar but were not reproduced here for the brevity of the paper.

CCT diagram of the oxidised slags

CCT diagram of the oxidised slags with different basicities was determined at different cooling rates and the results were shown in Fig. 14 to Fig. 16. In general, the crystallisation temperatures of precipitated phases increased with decreasing the cooling rate, which is in agreement with the experimental results by Wang *et al*. (2012). Wang *et al*. (2012) concluded that decreasing the cooling rate on BOF slag promoted full crystallisation of precipitated minerals. Besides, the crystallisation temperature of spinel phase (magnetite Fe_3O_4) increased while the temperature range for the crystallisation of spinel phase decreased with the increasing of slag basicity. For the oxidised slag with the

basicity of B=1.0 (Fig. 14), the difference in precipitation temperature between the primary phase of spinel (magnetite Fe_3O_4) and the second phase of melilite was observed to be very small and both phases formed at ~1200°C, and the slag liquid was observed to disappear at ~1000°C. This indicates that the temperature range for the crystallisation of spinel (magnetite Fe_3O_4) phase was ~200°C.

Fig. 15 is the CCT diagram for the oxidised slag with slag basicity of B=1.5 at different cooling rates from 10°C/min to 50°C/min. By increasing the cooling rate from 10°C/min to 50°C/min, the crystallisation temperature decreased from 1358°C to 1315°C for the first crystalline phase (Ca_2SiO_4) and from 1233°C to 1185°C for the spinel phase (magnetite Fe_3O_4). The disappearance of slag-liquid also decreased from 1115°C to 1060°C by increasing the cooling rate from 10°C/min to 50°C/min. It was noted that the crystallisation temperature range was ~120°C for the spinel phase (magnetite Fe_3O_4). For the oxidised slag with basicity of B=2.0, as illustrated in Fig. 16, by varying the cooling rate from 10°C/min to 50°C/min the crystallisation temperature varied from 1531°C to 1510°C for the first crystalline phase (Ca_2SiO_4), and from 1279°C to 1254°C for the spinel phase (Magnetite Fe_3O_4). The slag-liquid was observed to disappear at the temperature from 1221°C to 1205°C with varying the cooling rate from 10°C/min to 50°C/min. The temperature range for the crystallisation of spinel phase (magnetite Fe_3O_4) was ~50°C.

In comparison with the crystallisation behaviour of the oxidised slag (B=1.5), Fig. 17 shows the CCT diagram of the un-reacted slag (B=1.5) at different cooling rates. With increasing the cooling rate from 10°C/min to 50°C/min, the crystallisation temperature of the first crystalline phase (Ca_2SiO_4) decreased from 1451°C to 1390°C, which is much higher than the crystallisation temperature of 1358°C to 1315°C for the oxidised slag (Fig. 15). The second phase observed was monoxide with crystallisation temperature varying

from 1313°C to 1280°C. Unlike the oxidised slag (Fig. 15), no spinel phase (magnetite Fe_3O_4) was observed to precipitate from the un-reacted slag under Ar atmosphere. The disappearance of the slag-liquid occurred at the temperature from 1159°C to 1090°C with the cooling rate increasing from 10°C/min to 50°C/min. The difference in the crystallisation behaviour between the oxidised slag (under H_2O-Ar gas) and the un-reacted slag (under argon gas) clearly indicates the effect of slag-steam reaction on the slag chemistry and consequently its crystallisation behaviour. The CCT diagrams provide useful information for the crystallisation control (e.g. temperature control, cooling rate control) of the expected phase (e.g. magnetite Fe_3O_4) for different slags, which is valuable to design correct regimes for the recovery of valuable elements (Fe, Mn etc).

Recovery ratio of H_2 gas and maximum potential recovery ratio of iron oxide from oxidised slags

The different valences of iron in the oxidised and un-reacted slags were determined by chemical titration. As shown in Table 4, for the slags with same basicity, reacting the molten slag with H_2O-Ar gas at 1600°C substantially reduced the Fe^{2+} content and increased the Fe^{3+} content in the slag according to Eq. (1). The change in both the Fe^{2+} content and Fe^{3+} content between the oxidised slag and the un-reacted slag with same basicity increased with increasing the slag basicity from 1.0 to 2.0 although this change slightly decreased when the slag basicity increased from 1.5 to 2.0. This proves that the oxidation of FeO in the molten slag under the H_2O-Ar atmosphere did occur according to Eq. (1).

The recovery ratio of H_2 gas in the slag-steam reaction can be obtained by comparing the transformation ratio of Fe^{2+} to Fe^{3+} in the H_2O-Ar atmosphere and under Ar atmosphere according to Eq. (3).

$$\varepsilon_{H_2} = \frac{Fe_o^{3+} - Fe_u^{3+}}{TFe} \times 100\% \tag{3}$$

where ε_{H_2} is the recovery ratio of H_2 gas, %; Fe_o^{3+} and Fe_u^{3+} are the mass fraction of Fe^{3+} in the oxidised slag and un-reacted slag, %. Considering that the majority of Fe^{3+} in the oxidised slags existed in the form of Fe_3O_4, the maximum potential recovery of iron oxide in the oxidised slags by magnetic separation can be calculated by the mass fraction of Fe^{2+} and Fe^{3+} in Fe_3O_4. That is, the amount of Fe_3O_4 is stoichiometrically calculated based on the amount of Fe^{3+} in the slag according to Eq. (4).

$$\varepsilon_{\text{iron oxide}} = \frac{M_{Fe_3O_4} * (Fe_o^{3+} - Fe_u^{3+})}{M_{Fe_2O_3} * TFe} \times 100\% \tag{4}$$

where $\varepsilon_{\text{iron oxide}}$ is maximum potential recovery ratio of iron oxide in the oxidised slag, %; $M_{Fe_3O_4}$ and $M_{Fe_2O_3}$ are the molar mass of Fe_3O_4 and Fe_2O_3, g/mol. As a result, the recovery ratio of H_2 gas and the maximum potential recovery of iron oxide calculated *via* Eq. (3) and Eq. (4) are shown in Table 5. With increasing the slag basicity from 1.0 to 1.5 and 2.0, the recovery ratio of H_2 gas by reacting molten slag with H_2O-Ar gas varied from 12.6% to 23.7% and 22.6%, while the maximum potential recovery ratio of iron oxide changed from 18.3% to 34.4% and 32.8%. Semi-quantitative analysis of XRD results (Fig. 13) also showed that the reaction between molten slag (B=1.5) and H_2O-Ar gas increased the amount of magnetite phase (Fe_3O_4) by 31 %. Further study will be carried out to optimise the conditions for the recovery of H_2 gas and iron oxides. The depth of the reacted slag in contact with H_2O-Ar gas is one of the topics to be investigated. The fundamental knowledge generated from this study will provide necessary information for the engineering design to improve the recovery ratio of H_2 gas and iron oxides from the slags.

Conclusions

This research confirmed by both thermodynamic calculation and experimental study that the conversion of Fe^{2+} to Fe^{3+} took place by reacting molten steelmaking-type synthetic slag with H_2O-Ar gas. It provides fundamental knowledge for developing a novel process to recover energy (in the form of fuel gas) and materials (in the form of magnetite Fe_3O_4) from steelmaking slags.

The thermodynamic calculation showed that the accumulated amount of produced H_2 gas by reacting molten slag with H_2O-Ar gas increased with increasing the slag basicity (CaO/SiO_2) from 1.0 to 2.0. By combining the crystallisation behaviour observed by CSLM, the microstructure analysed by SEM-EDS and the phases present in the slag characterised by XRD, for the oxidised slag (B=1.5), the primary phase (Ca_2SiO_4) formed at 1358℃ and the second phase (Fe_3O_4) precipitated at 1233℃. CCT diagrams for different slags at different cooling rates indicate that the crystallisation temperatures of precipitated phases increased with decreasing the cooling rate, while the crystallisation temperature the spinel phase (magnetite Fe_3O_4) increased and the temperature range for the crystallisation of spinel phase decreased with the increasing of slag basicity.

The recovery ratio of H_2 gas and the maximum potential recovery ratio of iron oxide in the oxidised slags have been calculated by comparing the change in Fe^{3+} content between the slag reacting with H_2O-Ar gas and the slag under Ar gas only. With increasing the slag basicity from 1.0 to 1.5 and 2.0, the recovery ratio of H_2 was found to vary from 12.6% to 23.7% and 22.6%, and the maximum potential recovery ratio of iron oxide was found to change from 18.3% to 34.4% and 32.8%.

Acknowledgement

References

Barati, M., Esfahani, S. and Utigard, T.A. 2011. Energy recovery from high temperature slags, Energy 36, 5440-5449.

Bhattacharjee, D., Mukharjee, T. and Tathavadkar, V. 2007. Set-up for production of hydrogen gas by thermos-chemical decomposition of water using steel plant slag and waste materials, Tata Steel Limited, Publication No.: WO2007125537 A1.

Bhoi, B., Jouhari, A. K., Ray, H. S. and Misra, V. N. 2006. Smelting reduction reactions by solid carbon using induction furnace: Foaming behaviour and kinetics of FeO reduction in $CaO-SiO_2-FeO$ slag, Ironmaking & Steelmaking, 33, (3), 245-252.

Devia, V. S. and Gnanavel, B. K. 2014. Properties of concrete manufactured using steel slag, Procedia Engineering, 97, 95-104.

Fetters, K. L. and Chipman, J. 1941. Equilibria of liquid iron and slags of the system CaO-MgO-FeO-SiO$_2$. Trans. AIME, 145, 95-112.

Iacobescua, R. I., Koumpouri, D., Pontikesc, Y., Sabana. R. and Angelopoulos, G. N. 2011. Valorisation of electric arc furnace steel slag as raw material for low energy belite cements, J Hazard. Mater., 196, 287-294.

Kourounisa, S., Tsivilisa, S., Tsakiridisb, P. E., Papadimitrioub, G. D. and Tsiboukic, Z. 2007. Properties and hydration of blended cements with steelmaking slag, Cement Concrete Res., 37, (6), 815-822.

Lee, B. and Sohn, I. 2014. Review of innovative energy savings technology for the electric arc furnace, JOM, 66, (9), 1581-1594.

Makelaa, M., Watkins, G., Poykio, R., Nurmesniemiet, H. and Dahl, O. 2012. Utilization of steel, pulp and paper industry solid residues in forest soil amendment: Relevant physicochemical properties and heavy metal availability, J Hazard. Mater., 207-208, 21-27.

Matsuura, H. and Tsukihashi, F. 2012. Thermodynamic calculation of generation of H$_2$ gas by reaction between FeO in steelmaking slag and water vapor. ISIJ Int., 52, (8), 1503-1512.

Min, D. J., Han, J. W. and Chung, W. S. 1999. A study of the reduction rate of FeO in slag by solid carbon. Metall. Mater. Trans. B., 30B, 215-221.

Monaco, A., Lu, W. K. 1996. The properties of steel slag aggregates and their dependence on the melt shop practice, Steelmaking Conference Proceedings, 701-711, Pittsburgh, USA.

Mukherjee, T. and Bhattacharjee, D. 2007. A method for producing hydrogen and/or other gases from steel plant wastes and waste heat, Tata Steel Limited, Publication No.: WO2007036953 A1.

Nomura, T., Okinaka, N. and Akiyama, T. 2010. Technology of latent heat storage for high temperature application: a review. ISIJ Int., 50, (9), 1229-1239.

Pioro, L. S. and Pioro, I. L. 2004. Reprocessing of metallurgical slag into materials for the building industry, Waste Management, 24, 371-379.

Riley, A. L. and Mayes, W. M. 2015. Long-term evolution of highly alkaline steel slag drainage waters, Environ. Monit. Assess, 187, (463), DOI 10.1007/s10661-015-4693-1.

Rowe DM. 2006. Thermoelectric waste heat recovery as a renewable energy source, International Journal of Innovations in Energy Systems and Power, 1, (1), 13-23.

Sato, M., Matsuura, H. and Tsukihashi, F. 2012. Generation behaviour of H_2 gas by reaction between FeO-containing slag and H_2O-Ar gas, ISIJ Int., 52, (8), 1503-1512.

Semykina, A. 2012. The kinetics of oxidation of liquid FeO-MnO-CaO-SiO_2 slags in air, Metall. Mater. Trans. B, 43B, 56-63.

Semykina, A., Nakano, J., Sridhar, S., Shatokha, V. and Seetharaman, S. 2010a. Confocal microscopic studies on evolution of crystals during oxidation of the FeO-CaO-SiO_2-MnO slags, Metall. Mater. Trans. B, 41B, 940-945.

Semykina, A., Nakano, J., Sridhar, S., Shatokha, V. and Seetharaman, S. 2011b. Confocal scanning laser microscopy studies of crystal growth during oxidation of a liquid FeO-CaO-SiO_2 slag, Metall. Mater. Trans. B, 42B, 471-476.

Semykina, A. and Seetharaman, S. 2011a. Recovery of manganese ferrite in nanoform from the metallurgical slags. Metall. Mater. Trans. B, 42B, 2-4.

Semykina, A., Shatokha, V., Iwase, M. and Seetharaman, S. 2010b. Kinetics of oxidation of divalent iron to trivalent state in liquid FeO-CaO-SiO_2 slags, Metall. Mater. Trans. B, 41B, 1230-1239.

Teasdale, S. L. and Hayes, P. C. 2005. Kinetics of reduction of FeO from slag by graphite and coal chars, ISIJ int., 45, (5), 642-650.

Tossavainen, M., Engstrom, F., Yang, Q., Menad, N., Lidstrom Larsson, M. and Bjorkman, B. 2007. Characteristics of steel slag under different cooling conditions, Waste Management, 27, 1335-1344.

Turkdogan, E. T. and Pearson, J. 1953. Activities of constituents of iron and steelmaking slags. J. Iron Steel Inst., 173, 217-223.

Wang, D., Jiang, M., Liu, C., Min, Y., Cui, Y., Liu, J. and Zhang, Y. 2012. Enrichment of Fe-containing phases and recovery of iron and its oxides by magnetic separation from BOF slags, Steel Res. Int., 83, (2), 189-196.

Table captions:

Table 1 Chemical composition of synthetic slags;

Table 2 Chemical composition of master slags;

Table 3 EDS analysis of different phase areas in the quenched slag (B=1.5),

corresponding to Fig. 11(b) (Atomic Pct);

Table 4 Different valences of iron in the oxidised and un-reacted slags determined by

chemical titration;

Table 5 Recovery ratio of H_2 gas and iron oxide in oxidised slags.

Table 1 Chemical composition of synthetic slags

Basicity (B)[※]	Composition (Wt.%)						
	CaO	SiO$_2$	FeO	Al$_2$O$_3$	MgO	MnO	SUM
1.00	30.00	30.00	25.00	5.00	5.00	5.00	100.00
1.50	36.00	24.00	25.00	5.00	5.00	5.00	100.00
2.00	40.00	20.00	25.00	5.00	5.00	5.00	100.00

[※]In this work, basicity (B) is defined as CaO/SiO$_2$.

Table 2 Chemical composition of master slags

Basicity (B)[※]	Composition (Wt.%)						SUM
	CaO	SiO$_2$	FeO	Al$_2$O$_3$	MgO	MnO	
0.99	29.49	29.93	25.88	4.83	4.93	4.93	99.99
1.48	35.67	24.11	25.68	4.89	4.85	4.81	100.01
1.97	39.38	19.94	26.12	4.85	4.89	4.82	100.00

[※]In this work, basicity (B) is defined as CaO/SiO$_2$.

Table 3 EDS analysis of different phase areas in the oxidised slag (B=1.5), corresponding to Fig. 11(b) (Atomic Pct)

	Ca	Si	Fe	Al	Mg	Mn	O	SUM
P1	5.5	0.7	31.6	--	--	13.7	48.5	100
P2	6.8	0.6	30.4	--	--	12.7	49.6	100
P3	23.9	2.0	12.1	5.6	--	2.2	54.1	100
P4	24.0	2.2	12.5	5.4	--	2.3	53.6	100
P5	26.6	13.3	--	--	3.5	--	56.6	100
P6	26.6	13.2	0.4	--	3.5	0.9	55.4	100

--It indicates the amount of the elements is below the lower detection limit.

Table 4 Different valences of iron in the oxidised and un-reacted slags determined by chemical titration

	$Fe^{2+}/\%$	$TFe/\%$	$Fe^{3+}/\%$
B=1.0 (U)	14.9	26.2	11.3
B=1.0 (O)	11.6	26.2	14.6
B=1.5 (U)	12.6	25.7	13.1
B=1.5 (O)	6.5	25.7	19.2
B=2.0 (U)	12.8	23.9	11.1
B=2.0 (O)	7.4	23.9	16.5

U indicates the un-reacted slags, O indicates the oxidised slags.

Table 5 Recovery ratio of H_2 gas and iron oxide in oxidised slags

	Recovery ratio of H_2/%	Recovery ratio of iron oxide/%
B=1.0	12.6	18.3
B=1.5	23.7	34.4
B=2.0	22.6	32.8

Figure captions

Figure 1 Technological sheet to effectively utilize steelmaking slag;

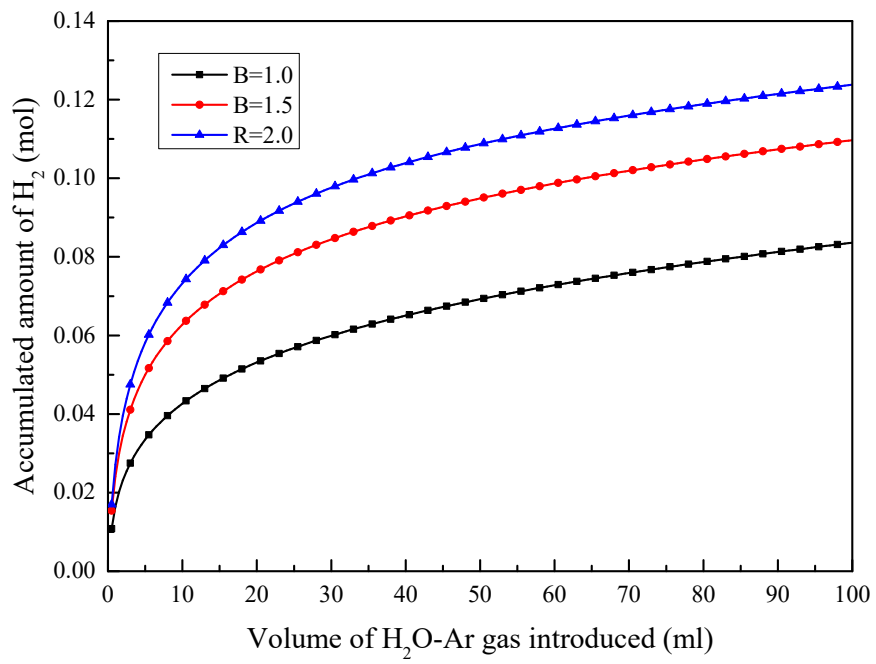Figure 2 Methodology of thermodynamic calculations by FactSage 7.0;

Figure 3 Change in accumulated amount of H_2 gas produced as a function of the volume of H_2O-Ar gas introduced and slag basicity;
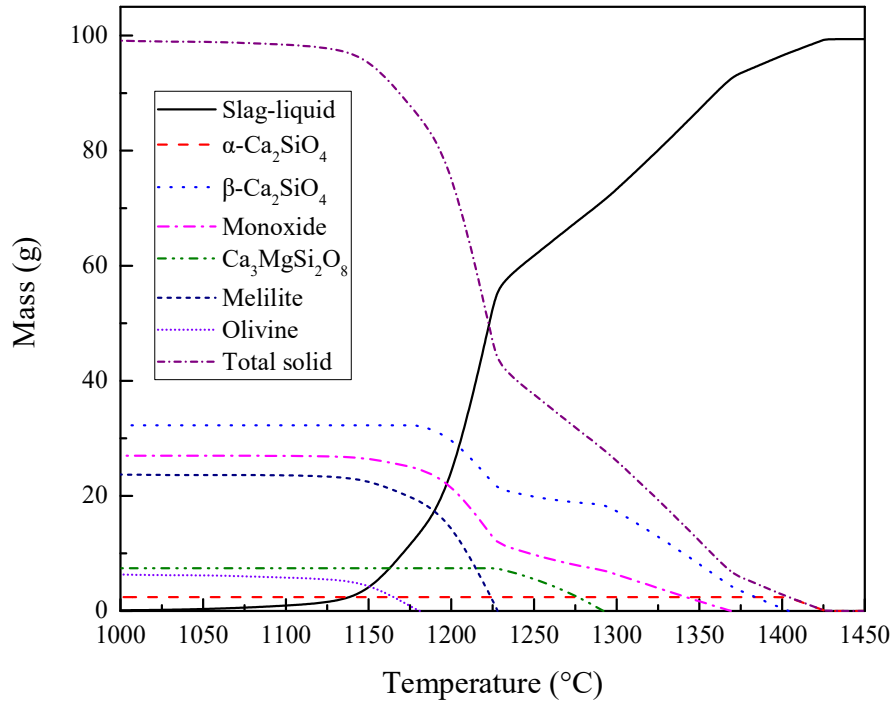
Figure 4 Change in accumulated amount of different phases precipitated from un-reacted slag (B=1.5);
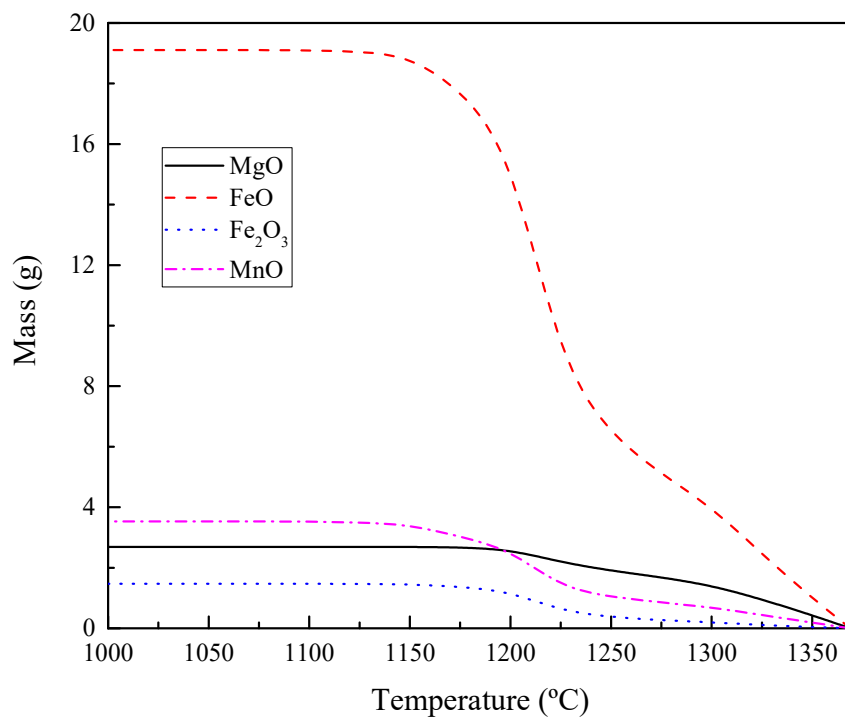
Figure 5 Constituents of monoxide phase generated from un-reacted slag (B=1.5);
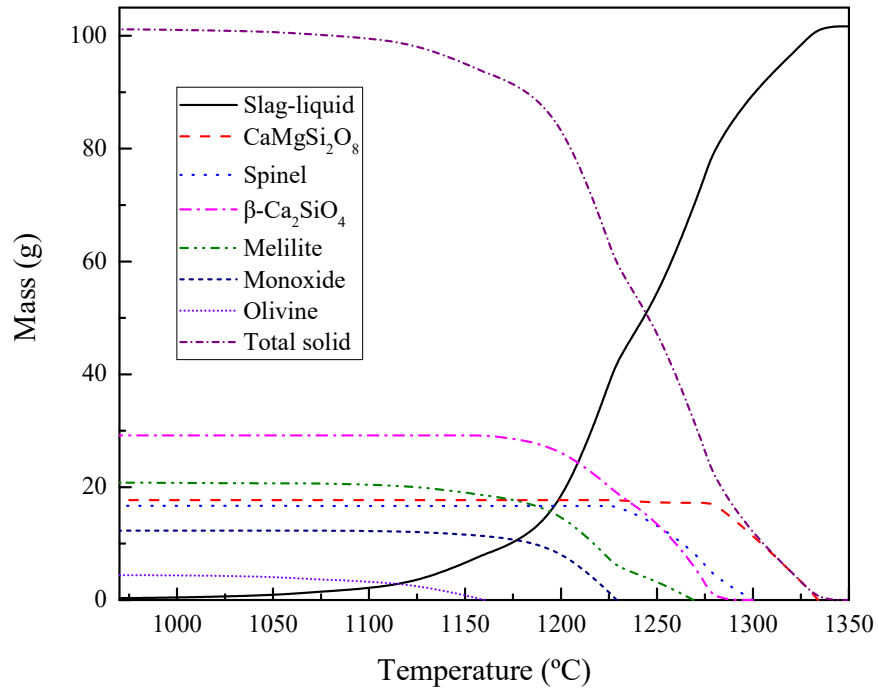
Figure 6 Change in accumulated amount of different phases precipitated from oxidised slag (B=1.5);
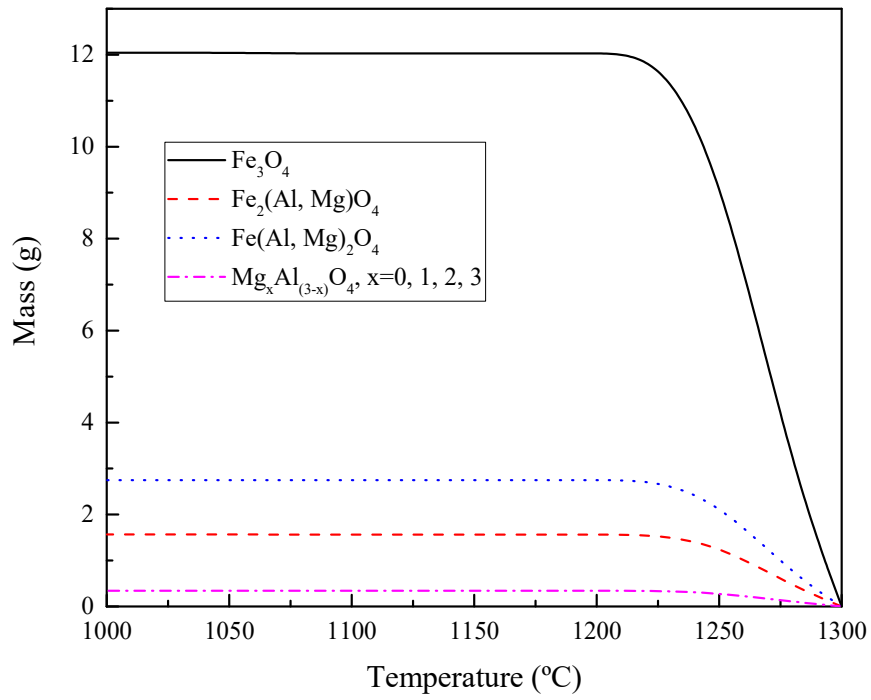
Figure 7 Constituents of spinel phase generated from oxidised slag (B=1.5);
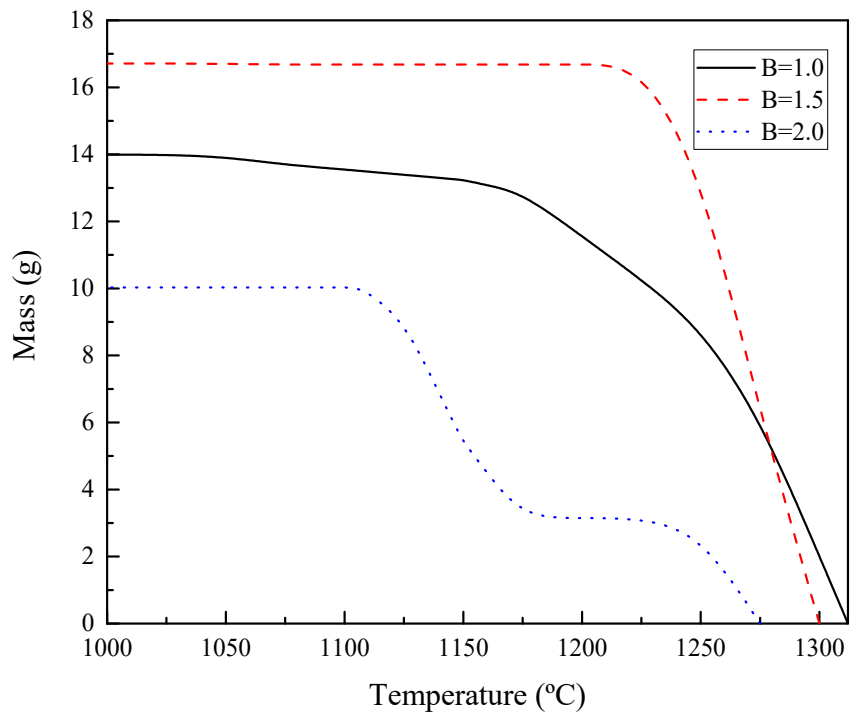
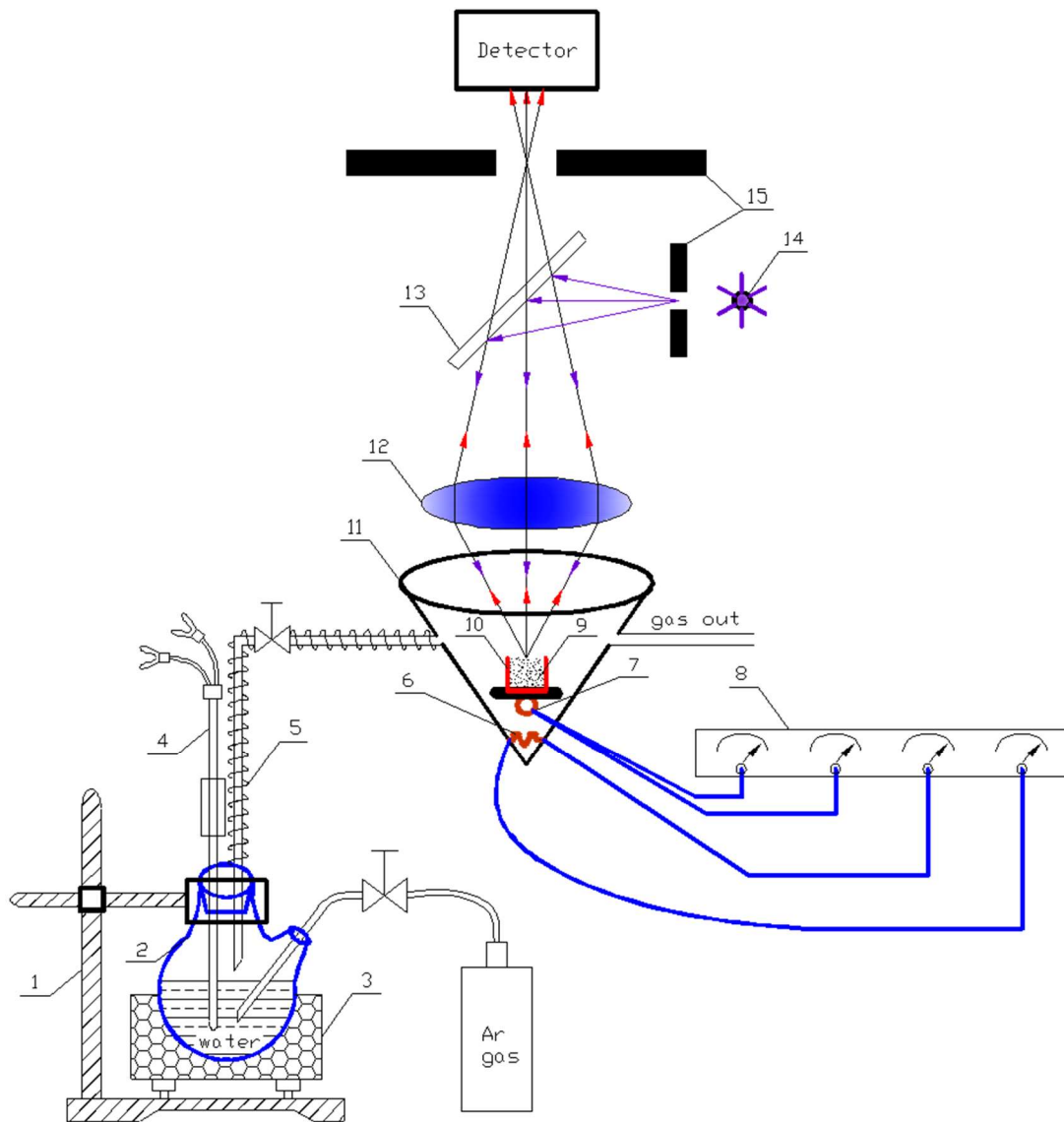Figure 8 Change in accumulated amount of spinel phase precipitated from oxidised slags with different basicities;
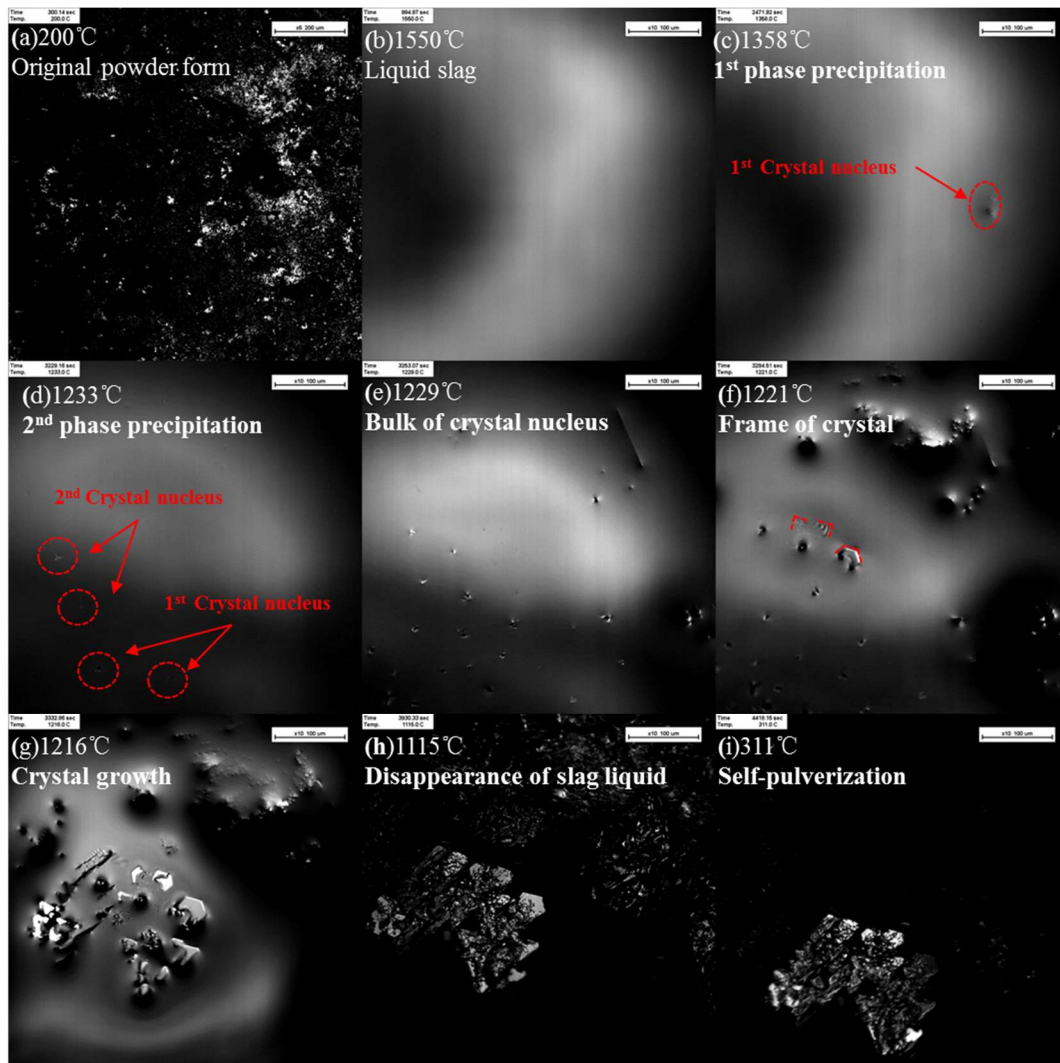
Figure 9 Schematic diagram of experimental apparatus;

Figure 10 Crystallisation behaviour observed by CSLM for oxidised slag (B=1.5) at the cooling rate of 10℃/min;

Figure 11 SEM photographs of oxidised slag (B=1.5) at the cooling rate of 10℃/min with different magnification factors: (a)500X, (b)3000X;

Figure 12 EDS map scanning of oxidised slag (B=1.5), corresponding to Fig. 11(b);

Figure 13 X-ray diffraction patterns of oxidised slag (B=1.5) and un-reacted slag (B=1.5);

Figure 14 CCT diagram of oxidised slag (B=1.0);

Figure 15 CCT diagram of oxidised slag (B=1.5);

Figure 16 CCT diagram of oxidised slag (B=2.0);

Figure 17 CCT diagram of un-reacted slag (B=1.5).

Figure 1 Technological sheet to effectively utilize steelmaking slag

Figure 2 Methodology of thermodynamic calculations by FactSage 7.0

Figure 3 Change in accumulated amount of H_2 gas produced as a function of the volume

of H_2O-Ar gas introduced and slag basicity

Figure 4 Change in accumulated amount of different phases precipitated from un-

reacted slag (B=1.5)

Figure 5 Constituents of monoxide phase generated from un-reacted slag (B=1.5)

Figure 6 Change in accumulated amount of different phases precipitated from oxidised

slag (B=1.5)

Figure 7 Constituents of spinel phase generated from oxidised slag (B=1.5)

Figure 8 Change in accumulated amount of spinel phase precipitated from oxidised

slags with different basicities

Figure 9 Schematic diagram of experimental apparatus

1: Retort stand; 2: Round-bottom flask; 3: Heating mantle; 4: Temperature probe; 5: Heater tape; 6: Halogen lamp; 7: Thermocouple; 8: Temperature controller; 9: Samples; 10: Platinum crucible; 11: Furnace chamber; 12: Lens; 13: Beam splitter; 14: He-Ne laser; 15: Pin hole

Figure 10 Crystallisation behaviour observed by CSLM for oxidised slag (B=1.5) at the cooling rate of 10℃/min

Figure 11 SEM photographs of oxidised slag (B=1.5) at the cooling rate of 10℃/min
with different magnification factors: (a) 500X; (b) 3000X

Figure 12 EDS map scanning of oxidised slag (B=1.5), corresponding to Fig. 11(b)

Figure 13 X-ray diffraction patterns of oxidised slag (B=1.5) and un-reacted slag
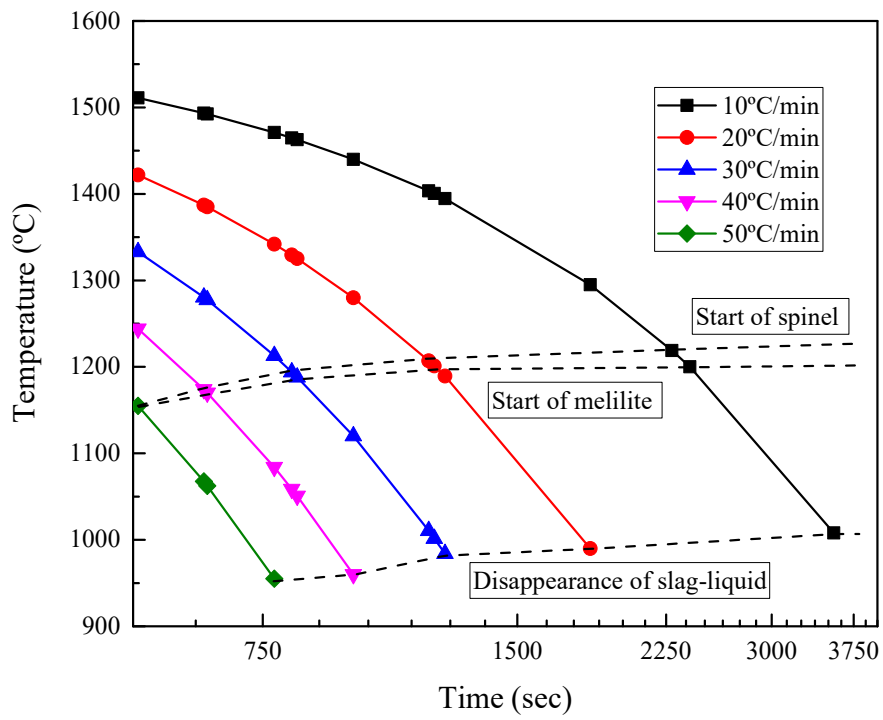
(B=1.5)

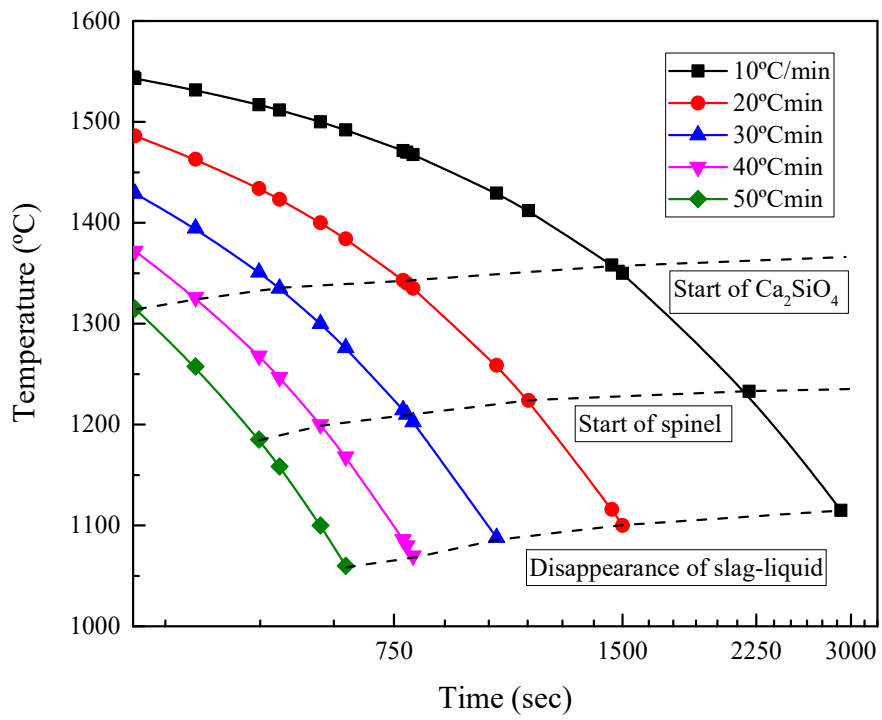Figure 14 CCT diagram of oxidised slag (B=1.0)

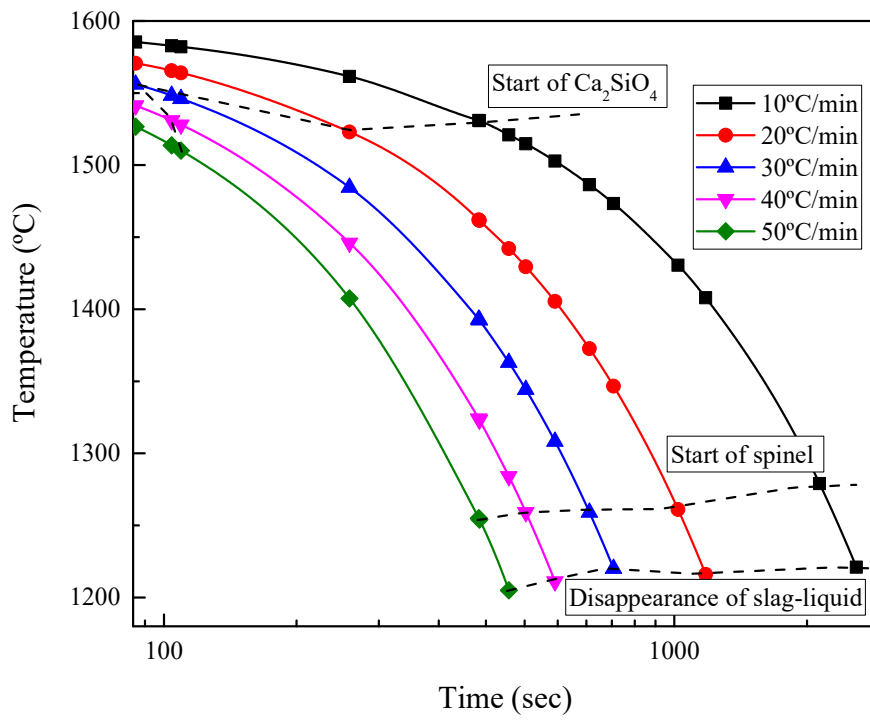Figure 15 CCT diagram of oxidised slag (B=1.5)
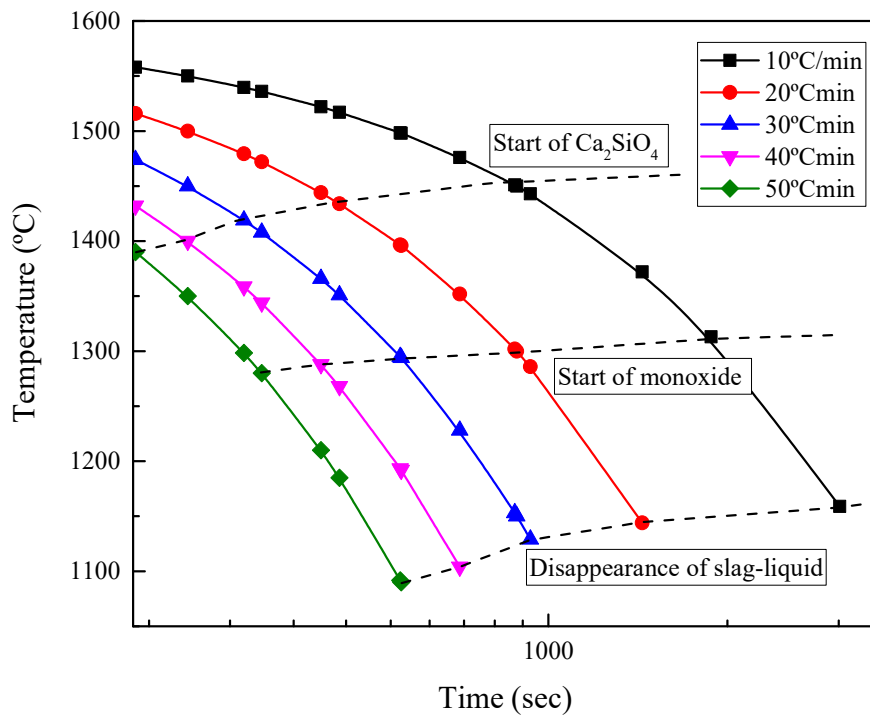
Figure 16 CCT diagram of oxidised slag (B=2.0)

Figure 17 CCT diagram of un-reacted slag (B=1.5)